processes

MDPI

Article

Mechanisms of Enhancing Tetracycline Oxidation in Wastewater by Ozone Micro-Nano Bubbles

Ruiyuan Li [1], Tianzhi Wang [1,2,*], Hangjia Zhao [1], Jinxin Chen [1], Ci Yang [1] and Fiallos Manuel [1]

[1] School of Environmental Science & Engineering, Tianjin University, Tianjin 300350, China
[2] Tianjin Key Laboratory of Pollution Prevention-Control and Carbon Sink Along Land-Sea Waters, Tianjin 300350, China
* Correspondence: wangtianzhi@tju.edu.cn

Abstract

To address the low efficiency of tetracycline (TC) ozonation caused by low ozone solubility, short aqueous half-life, and mass-transfer limitations, an ozone micro-nano bubble (O_3-MNBs) oxidation system was designed and systematically compared with conventional ozone sparging (Conv-O_3). Thus, this study assessed the bubble size distribution, zeta potential, ozone dissolution and decay behaviors in water, ·OH concentration, and TC oxidation products, elucidating the degradation pathways and underlying mechanisms enabled by O_3-MNBs. Relative to Conv-O_3, O_3-MNBs increased the steady-state dissolved ozone concentration by 2.57–4.33 times, reduced the ozone decay rate constant by 41.3%, and enhanced ·OH generation by 2.3 times. TC degradation in the O_3-MNB system exhibited a distinct two-stage kinetic behavior, following second-order kinetics in the initial period (0–30 s) and first-order kinetics thereafter (30–120 s). Accordingly, the TC removal efficiency of O_3-MNBs reached 96.25% within 120 s, which was 81.25% higher than that of Conv-O_3. Notably, TC removal under Conv-O_3 obeyed first-order kinetics throughout, with an apparent rate constant only 7.14% of that obtained with O_3-MNBs. These improvements were attributed to the sustained and efficient supply of oxidants, high dissolved ozone and ·OH radicals, promoting the conversion of TC intermediates toward low *m/z* small-molecule end products, with greater ring opening and skeletal fragmentation. Our findings suggest that the enhanced biodegradability results in a markedly reduced burden and environmental risk for subsequent biological or advanced treatment processes. Therefore, this study highlights the potential of O_3-MNBs to enhance ozone utilization and oxidation intensity, providing mechanistic insights and technical support for rapid pretreatment of antibiotic-containing wastewater.

Keywords: ozone micro-nano-bubbles; tetracycline degradation; high dissolved ozone concentration; reaction kinetics; degradation pathways

Check for updates

Academic Editor: José A. Peres

Received: 28 February 2026
Revised: 14 March 2026
Accepted: 26 March 2026
Published: 28 March 2026

Copyright: © 2026 by the authors. Licensee MDPI, Basel, Switzerland. This article is an open access article distributed under the terms and conditions of the Creative Commons Attribution (CC BY) license.

1. Introduction

With socioeconomic development and increasing demand for antibiotics, substantial quantities of antibiotics are discharged into surface waters via wastewater treatment plant effluents or untreated wastewater [1]. It is calculated that global rivers receive approximately 9500 tons of antibiotics annually from human use (about 31% of total antibiotic consumption) [2], making antibiotic contamination a worldwide environmental challenge. For instance, in South Asian countries, such as India and Pakistan, the coexistence of rapidly increasing antibiotic usage and insufficient wastewater-treatment infrastructure has led

to antibiotic concentrations in natural waters. As a result, this wastewater level ($mg \cdot L^{-1}$) has exceeded the high-risk threshold, ranking the region among the most severely affected areas globally [3,4]. In China, antibiotics have been detected in some rivers in western regions at concentrations ranging from several hundred to several thousand $ng \cdot L^{-1}$ [5,6]. Although the European Union and other developed regions have strengthened regulatory control over pharmaceutical micropollutants through legislation, existing treatment technologies face limitations resulting in long-term accumulation of antibiotics in aquatic environments, with concentrations reaching tens of $ng \cdot L^{-1}$ [7]. The presence of antibiotics can severely disrupt the normal metabolism of aquatic microorganisms and destabilize microbial community structures, thereby impairing ecosystem function. Moreover, certain antibiotics can enter the human body through multiple pathways (e.g., drinking water and aquatic products), posing substantial risks to human health [8,9]. Among these antibiotics, tetracycline (TC) deserves particular concern because it is widely detected in aquatic environments and can persist in water, sediment, and wastewater matrices. Recent studies have shown that TC contamination may exert ecological toxicity on non-target organisms and microbial communities, while also promoting the enrichment and transfer of antibiotic resistance genes even at environmentally relevant concentrations [10,11]. Consequently, the efficient removal and control of antibiotics in water has become an urgent global priority.

To date, the major classes of antibiotics identified in aquatic environments include β-lactams, macrolides, aminoglycosides, tetracyclines, chloramphenicols, and quinolones, among which tetracyclines are particularly widespread and often detected at relatively high levels [12]. As reported by a survey, 19 sites along the Huangpu River in China recorded a median tetracycline concentration of 36.71 $ng \cdot L^{-1}$ [13]. Similarly, in the United States, 139 rivers across 30 states detected 21 antibiotics (e.g., tetracyclines, sulfonamides, and lincomycin) with concentrations up to 1.0 $\mu g \cdot L^{-1}$ [14]. Several studies have demonstrated that even at sub-inhibitory concentrations (commonly defined as <1 $\mu g \cdot mL^{-1}$, and even as low as the $ng \cdot L^{-1}$ level), tetracycline can act as a robust environmental selective pressure, continuously driving the emergence and enrichment of antibiotic resistance genes within microbial communities [15]. Due to its chemical stability, tetracycline can persist in natural waters for extended periods, posing a significant risk to aquatic ecosystems [16]. In addition, tetracycline exposure is associated with adverse health effects, including gastrointestinal disturbances, allergic reactions, tooth discoloration, and hepatic/renal impairment. For example, severe diarrhea may occur upon exposure to tetracycline, because it suppresses not only pathogenic bacteria but also a broad range of sensitive commensal gut microbiota [17]. Therefore, developing efficient strategies for tetracycline removal from wastewater has become a key scientific challenge in the field of antibiotic pollution control.

Current mainstream wastewater treatment processes (e.g., anaerobic–aerobic combined systems) typically achieve less than 40% removal efficiency for tetracycline due to its stable molecular structure and slow adsorption in the sludge [18,19]. While conventional anaerobic/anoxic/oxic (A^2/O) processes have reported more than 80% of tetracycline partitioning into waste-activated sludge, this poses a risk of secondary release during subsequent sludge handling and disposal [18]. In contrast, advanced oxidation processes (AOPs) can efficiently degrade and even mineralize tetracycline via the generation of hydroxyl radicals (·OH), showing clear advantages [20]. Among them, photocatalytic oxidation can achieve a higher degradation (>90%) under UV irradiation in the presence of TiO_2 [21], although it depends on the light input and suffers from catalyst recovery challenges. The Fenton process is effective under acidic conditions but produces iron-containing sludge [20], which incurs relatively high operating costs, and has a narrow functional pH window. Physicochemical approaches (i.e., membrane separation and activated carbon adsorption) are further limited in large-scale applications via high investment, reduced capacity, and secondary waste generation [21].

As an essential branch of AOPs, the ozonation process has shown potential because of its strong oxidizing power, rapid reaction kinetics, and the absence of secondary sludge generation. In practice, tetracycline removal by ozonation is conducted through (i) direct oxidation by molecular ozone and (ii) indirect oxidation by ·OH formed under alkaline conditions [22]. However, its performance is often limited by low ozone solubility, short aqueous half-life, and poor gas–liquid mass transfer efficiency. In conventional bubble contactors, these factors can lead to low ozone utilization efficiency and insufficient dissolved ozone availability in the liquid phase, thereby restricting the effective oxidation of refractory pollutants. Moreover, although tetracycline can be rapidly transformed by ozonation, deep mineralization is often limited and transformation products with altered toxicity may still be formed [23,24]. To address these limitations, catalytic ozonation has emerged as a research hotspot, where metal oxides or supported catalysts (e.g., Fe_3O_4-CeO_X/AC@ZrO_2 or SBC-LDH) promote ·OH generation and enhance degradation and mineralization [25]. However, current approaches remain highly catalyst-dependent, and issues such as catalyst stability, synthesis complexity, and preparation cost can compromise overall efficiency [26]. For instance, Fe–Mn/AC catalysts prepared via impregnation–calcination can substantially improve degradation under optimized conditions, although they are restrained by stimulus dosage, pH, and other operating parameters [27]. Meanwhile, sophisticated core–shell designs (e.g., Fe_3O_4-CeO_X/AC@ZrO_2) improve stability but significantly increase fabrication difficulty and cost [26]. Therefore, to ensure sustained, efficient, and stable ozonation of tetracycline in water, there is an urgent need to develop novel solutions that simultaneously deliver enhanced mass transfer and oxidation capability.

Micro-nano bubble (MNB) technology has emerged as a promising approach to overcome the mass-transfer limitations of ozonation. Compared with conventional bubbles, MNB (typically ranging from tens of micrometers to hundreds of nanometers in diameter) exhibit an extremely low rising velocity. Together with their generally negatively charged surfaces, which suppress bubble coalescence, MNBs can remain suspended in the liquid phase for markedly prolonged periods (up to several hours) [28]. Additionally, their large specific interfacial area (>1000 $m^2 \cdot m^{-3}$) significantly increases the gas–liquid contact interface [29]. More importantly, the high Laplace pressure inside MNBs (up to several atmospheres) substantially enhances the supersaturated solubility of gases and the driving force for mass transfer [28,30]. Thus, upon collapse in the liquid phase, the rapid disappearance of the gas–liquid interface can generate localized high temperature and pressure as well as intense shear, accompanied by the formation of reactive species such as hydroxyl radicals (·OH) [31,32]. These features endow MNB technology with considerable potential for intensifying gas dissolution and mass transfer. When coupled with ozone oxidation, ozone micro-nano-bubbles (O_3-MNBs) can increase ozone solubility and residence time in water, thereby improving ozone utilization efficiency [30]. Furthermore, the collapse of MNBs may create localized high-temperature/high-pressure microenvironments, generating abundant radical formation, which can further enhance the oxidative capacity of ozone [30,33]. Based on this principle, this technology can improve ozonation efficiency for tetracycline, providing a robust technical framework to address challenges of tetracycline-containing wastewater treatment.

Recent studies have demonstrated that bubble-enhanced ozonation can substantially improve ozone utilization and pollutant removal, but the reported systems and research focuses remain quite different. For example, Wang et al. employed an ultrafine-bubble compressor to assist tetracycline ozonation and confirmed that finer bubbles can markedly improve dissolved ozone availability and tetracycline degradation efficiency [34]. Tang et al. further showed that micronano-bubble ozonation is effective as a pretreatment technology for raw oxytetracycline production wastewater, highlighting its practical value

for high-strength antibiotic wastewater [35]. More recently, Zhao et al. reported that ozone micro-nano bubbles exhibited remarkable effectiveness for tetracycline removal and provided important evidence for the environmental implications and degradation pathway evolution of TC during O_3-MNB treatment [36]. In addition, Yang et al. demonstrated that ozone micro-bubble aeration can significantly enhance disinfection performance while reducing ozone dosage, indicating that microbubble-assisted ozonation may improve oxidant utilization efficiency in water treatment [37]. Compared with these recent studies, the present work places greater emphasis on the integrated relationship among ozone retention and decay behavior, aqueous-phase oxidant availability, two-stage degradation kinetics, and the evolution of transformation products during TC oxidation. Therefore, this study extends current O_3-MNB research from performance verification toward a more systematic mechanistic understanding of tetracycline degradation in water.

This study addressed these limitations by assessing the tetracycline degradation kinetics and removal performance in an O_3-MNBs system under varied operating conditions, elucidating how MNB technology enhances ozonation. Degradation intermediates were identified using liquid chromatography–mass spectrometry (LC–MS), and tetracycline transformation pathways were analyzed to clarify the removal routes and response mechanism for the O_3-MNBs-enhanced degradation. Overall, this study aims to provide a solid theoretical basis and technical support for the practical application of MNBs technology in advanced wastewater treatment and the control of antibiotic pollution.

2. Materials and Methods

2.1. Experimental System for Tetracycline Degradation by O_3-MNBs

Experimental analyses were performed in the O_3-MNBs Laboratory at the School of Environmental Science and Engineering, Tianjin University. Thus, we designed a TC removal system to investigate the degradation mechanism of TC by O_3-MNBs, as shown in Figure 1.

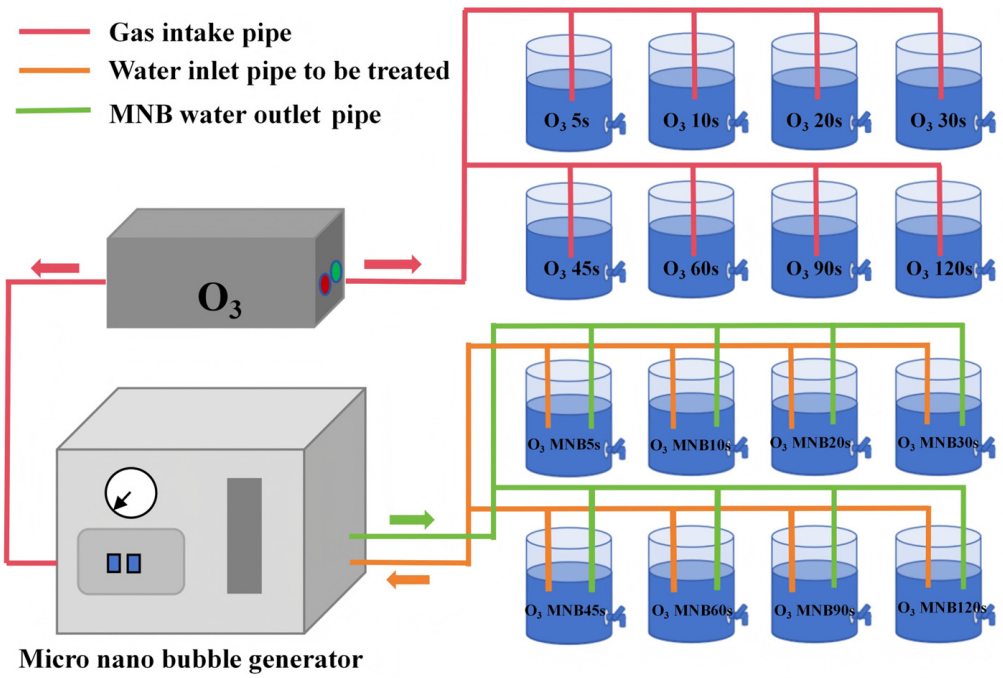

Figure 1. TC degradation system scheme.

The system consisted of an ozone generator, an MNB generator, and a reaction vessel, setting treated water at 5 L. Additionally, this study incorporated two ozone aeration modes

for comparison. Ozone was generated by an ozone generator (model WTS-SCLL, with a nominal ozone production rate of 50 g/h), and the ozone gas (i.e., the inlet flow to the micro-nano bubble generator) was introduced into the micro-nano bubble generator to produce bubbles with diameters ranging from 50 to 1200 nm. The influent flow rate was set at 10 $L \cdot min^{-1}$, treating the water in a fixed batch for 2 min. During treatment, samples were collected at 0, 5, 10, 20, 30, 45, 60, 90, and 120 s, and $Na_2S_2O_3$ was immediately added to quench residual oxidants and terminate the reaction. Unless otherwise stated, the baseline experimental conditions were as follows: treated water volume = 5 L, initial TC concentration = 40 $mg \cdot L^{-1}$, initial solution pH = 7, gas inlet flow rate = 1 $L \cdot min^{-1}$, and reaction time = 120 s. Ozone was generated by the ozone generator (WTS-SCLL, nominal ozone production rate: 50 $g \cdot h^{-1}$), and the ozone input condition was controlled by the gas flow rate and aeration time. All experiments were conducted at room temperature. The details regarding all the chemical substances used in this study and the mechanism of bubble formation can be found in the Supplementary Information.

2.2. Testing Items

(1) Characterization of micro-nano-bubbles

The size distribution and zeta potential of MNBs were measured using a nanoparticle size and zeta potential analyzer (Malvern Panalytical ZS90, Malvern Panalytical Ltd., Malvern, Worcestershire, UK). Microscopic observation using a biological microscope (Phoenix XSP-36-1600X, Phenix Optics Co., Ltd., Shangrao, Jiangxi, China), followed by image-based counting and calculation, was used to determine the concentration of optically detectable bubbles.

(2) Hydroxyl radicals (·OH)

p-Hydroxybenzoic acid (4-HBA) was employed as an ·OH probe. ·OH reacts with 4-HBA via hydrogen abstraction/substitution at the ortho position relative to the hydroxyl group, yielding 3,4-dihydroxybenzoic acid (3,4-DHBA) as the hydroxylated product. The concentration of 3,4-DHBA was estimated by high-performance liquid chromatography (HPLC; Dionex Ultimate 3000, Thermo Fisher Scientific, Sunnyvale, CA, USA) equipped with a UV detector, and the ·OH concentration generated in the system was calculated accordingly.

(3) Total organic carbon (TOC)

TOC in ozonated water samples was measured using a TOC analyzer (TOC-LCPN, Shimadzu Corporation, Kyoto, Japan).

(4) Tetracycline concentration

Using HPLC, the TC concentration was quantified. A C18 column (250 mm × 4.6 mm, 5 μm) was used with a mobile phase consisting of 0.01 $mol \cdot L^{-1}$ oxalic acid solution and acetonitrile (69:31, v/v) at a flow rate of 1.0 $mL \cdot min^{-1}$. The detection wavelength was set at 355 nm, the column temperature at 35 °C, and the injection volume was 20 μL. A calibration curve was employed using TC standard solutions at different concentrations. After appropriate pretreatment, samples were analyzed under identical conditions, and TC concentrations were calculated from peak areas using the calibration curve.

(5) Dissolved ozone concentration in water

By continuous analysis, the aqueous ozone concentration was monitored using a UV ozone analyzer (RD-O_3-1, Ruidezhi Innovation Technology (Tianjin) Co., Ltd., Tianjin, China) (254 nm), calibrated with standard ozone gas. Water samples introduced into a flow-through cell at 100–200 $mL \cdot min^{-1}$. Absorbance was recorded continuously and converted to ozone concentration.

(6) Transformation products of tetracycline

Transformation products formed during ozonation were analyzed using a triple-quadrupole mass spectrometer (LCMS-8045, Shimadzu Corporation, Kyoto, Japan). The HPLC–UV detector was set at 280 and 355 nm to monitor the TC oxidation products. Under positive ion mode (ESI+), with the precursor ion at *m/z* 445.1 and the product ion at *m/z* 410.0, a fragmentation voltage of 100 V, a collision energy of 20 V, nitrogen (N_2) as the nebulizing/drying gas (350 °C, 8 L·min^{-1}), new signals were detected in MS^2 scan mode and their *m/z* values were obtained. Following that assessment, we further analyzed the resulting degradation mechanisms.

3. Results and Analysis

3.1. Effect of Ozone Gas Flow Rate on Aqueous Ozone Retention Characteristics

The variations in aqueous ozone retention characteristics under different gas inlet flow rates are shown in Figure 2. As illustrated in Figure 2a, the O_3-MNB water produced in this system exhibited a bubble number concentration of (5.25–7.17) × 10^7 mL^{-1}. The bubble size was predominantly distributed within 50–1200 nm (Figure 2d), accounting for more than 95% of the total population. By contrast, under conventional ozone aeration, the bubble concentration in water was only ~1%, which is deficient compared with the bubble production in O_3-MNB water. In addition, the zeta potential of the O_3-MNB water ranged from −4.71 to −13.65 mV (Figure 2b), while under conventional aeration, the zeta potential was null. The temporal variation in zeta potential may be associated with the dynamic evolution of bubble interfacial properties, including possible changes in bubble size distribution, surface ion enrichment, and bubble collapse and dissolution. These findings indicate that a large amount of anions was enriched on the bubble surface [30]; which can generate radicals in situ during bubble collapse [38]. At the same time, this process led to an average radical concentration of 21.49 μmol·L^{-1} in the O_3-MNB water (Figure 2c), which was 117% higher than that in the conventional ozone-aerated water.

Furthermore, by increasing aeration time, the dissolved ozone concentrations under both aeration modes exhibited a consistent three-stage trend, including a slow increase (0–40 s), followed by the rapid rise (40–300 s) and dynamic stabilization (300–630 s) (Figure 2e). During the slow-increase stage, the ozone accumulation rates were comparable for the two aeration modes, ranging from 0.57 to 0.97 mg·L^{-1}·min^{-1}. During the rapid-rise stage, the ozone accumulation rate in the O_3-MNB water reached 4.22 mg·L^{-1}·min^{-1}, which was 147.25% higher than that under conventional ozone aeration. The dissolved ozone concentration reached its maximum at 480 s, with the O_3-MNB water achieving a peak value of 27.9 mg·L^{-1}, which was 85.50% higher than that obtained by conventional ozone aeration at the same gas flow rate.

After the aeration process stopped, the dissolved ozone reached its peak, while under conventional aeration, the dissolved ozone decreased immediately. Thus, the O_3-MNBs water continued to increase by 20.1% within the first 60 s after aeration cessation (Figure 2f), rising from 13.04 mg·L^{-1} to 15.66 mg·L^{-1}, and then began to decline. Moreover, the ozone decay processes after aeration cessation under both aeration modes followed first-order kinetics. The ozone decay rate under the O_3-MNB condition was 0.023 mg·L^{-1}·min^{-1}, which was 39.57% slower than that under conventional aeration. By the end of the observation period (25 min after aeration cessation), the average dissolved ozone concentration in the O_3-MNBswater remained at 4.69 mg·L^{-1}, corresponding to 44.82% of its maximum value, whereas that under conventional aeration was 1.22 mg·L^{-1} (only 26.17% of that in the O_3-MNB water).

Across varying gas inlet flow rates, the O_3-MNB system consistently exhibited markedly superior overall performance compared with conventional ozone aeration. By

increasing the gas inlet flow rate, the bubble number concentration in the O_3-MNB water remained stable at 10^7 mL^{-1}, while the bubble size showed an increasing trend. At a gas inlet flow rate of 1.5 $L \cdot min^{-1}$, the saturated dissolved ozone concentration and hydroxyl radical (·OH) generation in water reached their maxima, i.e., 27.9 $mg \cdot L^{-1}$ and 25.61 μM, respectively. These values were higher than those obtained at gas inlet flow rates of 0.5, 1.0, and 2.0 $L \cdot min^{-1}$ by 31.42%, 7.70%, and 3.02% for the saturated ozone concentration, and by 16.43%, 10.24%, and 5.11% for ·OH generation, respectively. The gas inlet flow rate exerted no significant effect on the zeta potential of the bubble water. It should be noted that the increase in ·OH concentration did not scale directly with the apparent bubble concentration. This result indicates that ·OH formation was governed not only by bubble number, but also by dissolved ozone concentration, bubble size, and interfacial processes. Therefore, although conventional ozone aeration produced fewer bubbles, it still generated measurable ·OH, while O_3-MNBs showed higher ·OH production due to more favorable ozone retention and interfacial activation.

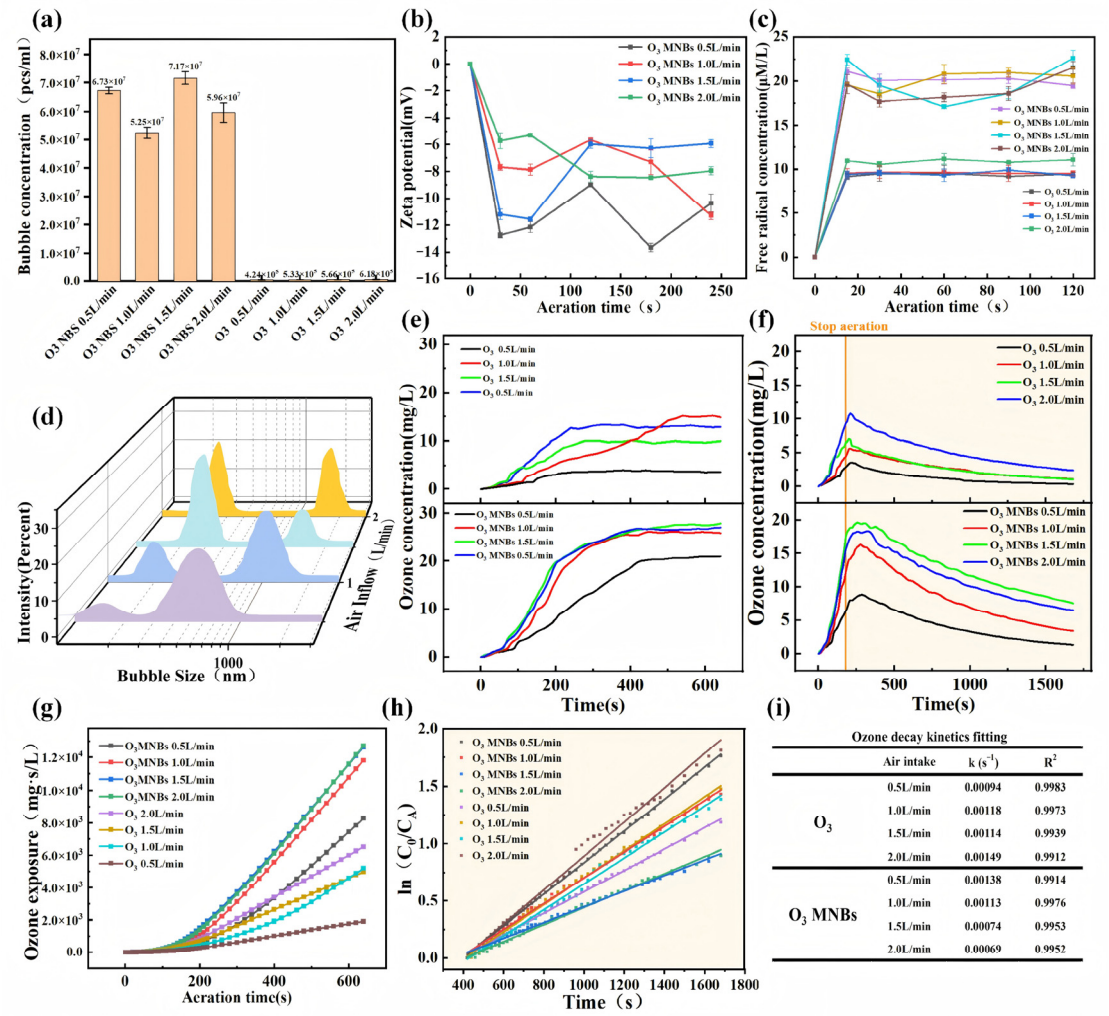

Figure 2. Bubble characteristics and ozone behavior in water under different aeration conditions. (**a**) Concentration of bubbles in water under different aeration conditions. (**b**) Zeta potential in water under different aeration conditions. (**c**) Concentration of hydroxyl radicals in water under different aeration conditions. (**d**) Bubble Size Distribution in Water under Different Aeration Conditions. (**e**) Changes in ozone concentration in water under different aeration conditions. (**f**) Ozone Concentration Decay Experiment in Water under Different Aeration Conditions. (**g**) Ozone exposure under different aeration conditions. (**h**) Kinetic modeling of ozone decay in water under different aeration conditions. (**i**) Ozone decay kinetics fitting results.

3.2. Effect of O_3-MNBs on Tetracycline Degradation Efficiency

The treatment execution with ozone for TC degradation was at different concentrations under two aeration modes. As shown in Figure 3, the removal efficiency and removal rate of the O_3-MNB system were significantly higher than those of conventional O_3 aeration. With increasing reaction time, TC degradation in the O_3-MNBs system exhibited two distinct phases, i.e., an extremely rapid degradation phase followed by a rapid degradation phase. Specifically, within 0–30 s, TC degradation by O_3-MNBs followed second-order kinetics, with the second-order rate constant (K_2) of 1.06×10^{-3}–5.93×10^{-3} $mol^{-1} \cdot L \cdot s^{-1}$. From 30 to 120 s, TC degradation by O_3-MNBs followed first-order kinetics, with the first-order rate constant (K_1) of 9.21×10^{-3}–2.28×10^{-2} s^{-1}. In contrast, under conventional ozone aeration, the entire TC degradation process followed first-order kinetics, with K_1 from 1.13×10^{-3} to 1.62×10^{-3} s^{-1}, which was only 7.14% of that in the O_3-MNB treatment. Consequently, at 30 s, the TC removal efficiency achieved by O_3-MNBs was 85.78%, which was 85.75% higher than that under conventional ozone aeration; at 120 s, the TC removal efficiency of O_3-MNBs reached 96.25%, which was 81.25% higher than that of the standard method.

As the initial TC concentration increased, the removal efficiency and reaction rate of TC degradation by O_3-MNBs showed a decreasing trend. The 20 $mg \cdot L^{-1}$ group exhibited the highest removal efficiency and the largest kinetic constants (K_2 and K_1), reaching 97.26%, 5.74×10^{-3} $mol^{-1} \cdot L \cdot s^{-1}$, and 2.28×10^{-2} s^{-1}, respectively (Figure 3a, Table 1). These values were higher than those obtained for the 40, 60, 80, and 100 $mg \cdot L^{-1}$ groups by 2.58%, 4.95%, 4.55%, and 4.23% in removal efficiency; by 121.62%, 189.90%, 210.27%, and 441.51% in K_2; and by 52.61%, 116.03%, 147.23%, and 86.18% in K_1, respectively. Notably, although high initial TC concentrations reduced the degradation efficiency of O_3-MNBs, the total amount of TC removed increased substantially (when the initial concentration increased from 20 to 100 $mg \cdot L^{-1}$, the total removed amount increased from 19.45 to 93.30 $mg \cdot L^{-1}$). These results indicate that O_3-MNBs can rapidly degrade more than 90% of TC under high pollution loads and achieve a complete removal rate (with a maximum removal efficiency exceeding 97%) under low pollution loads.

Under different gas inlet flow rates, the TC removal performance of the O_3-MNB system exhibited a non-monotonic dependence. Across air inflow conditions, the group treatment at 1.5 $L \cdot min^{-1}$ achieved the highest performance, with a removal efficiency of 99.00% and kinetic constants K_2 and K_1 of 5.93×10^{-3} $mol^{-1} \cdot L \cdot s^{-1}$ and 2.83×10^{-2} s^{-1}, respectively (Figure 3b, Table 1). Compared with the 0.5, 1.0, and 2.0 $L \cdot min^{-1}$ groups, these values were higher by 4.19%, 231.28%, and 2.58% for removal efficiency; by 5.28%, 128.96%, and 89.48% for K_2; and by 1.79%, 27.53%, and 59.10% for K_1, respectively.

Across varying initial pH conditions, the TC degradation performance of the O_3-MNBs system exhibited a nonlinear dependence; thus, environments under strong acidic and alkaline conditions resulted in higher removal efficiencies. This removal efficiency was achieved at a pH of 3, reaching 98.83%, which was higher than those at a pH of 5, 7, 9, and 11 by 1.45%, 4.81%, 1.80%, and 1.25%, respectively. Notably, the initial-stage (0–30 s) kinetic behavior differed markedly from the final degradation efficiency: at a pH of 9, the second-order rate constant K_2 was 4.07×10^{-3} $mol^{-1} \cdot L \cdot s^{-1}$ (Table 1), which was higher than those at pHs of 3, 5, 7, and 11 by 29.62%, 80.09%, 57.14%, and 180.69%, respectively. Our findings suggest that under mildly alkaline conditions, ozone may rapidly decompose to generate highly reactive radicals, which trigger an explosive oxidation reaction. In the subsequent reaction stage (30–120 s), the first-order rate constant K_1 at pH = 3 reached 3.07×10^{-2} s^{-1}, which was higher than those at pHs of 5, 7, 9, and 11 by 21.28%, 105.89%, 69.16%, and 1.08%, respectively.

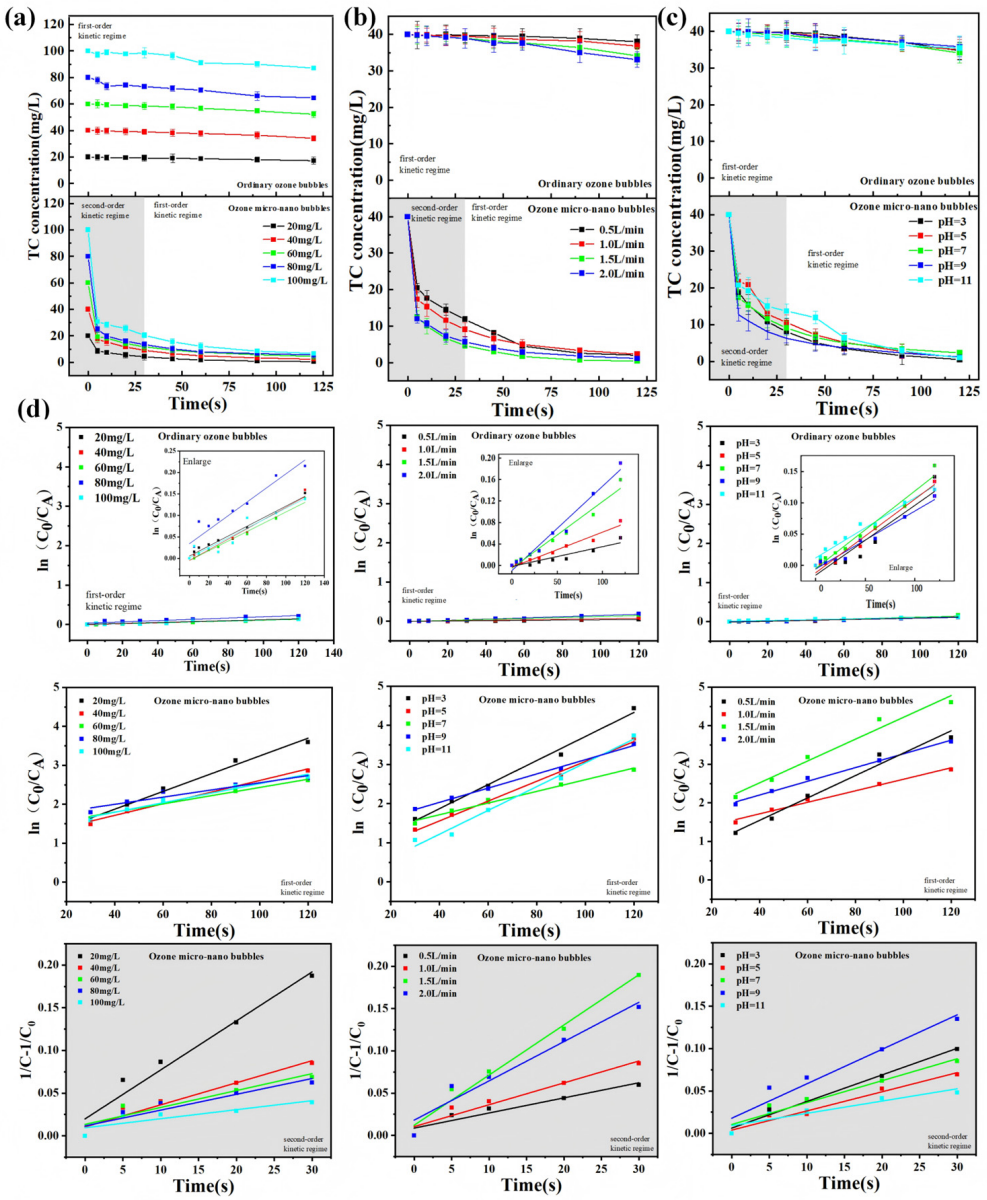

Figure 3. Degradation of Tetracycline by ozone under different conditions. (**a**) Degradation of Tetracycline by Two Types of Ozone with Different Initial Concentrations. (**b**) Degradation of Tetracycline by Two Types of Ozone under Different Air Intake Rates. (**c**) Degradation of tetracycline by two types of ozone at different pH levels. (**d**) Kinetic fitting results of tetracycline degradation by two types of ozone under different conditions.

Table 1. Kinetic fitting results.

Conditions		Ozone Micro-Nano Bubbles				Ordinary Ozone Bubbles	
		Second-Order Kinetic (0–30 s)		First-Order Kinetic (30–120 s)		First-Order Kinetic (0–120 s)	
		K_2 ($mol^{-1}·L·s^{-1}$)	R^2	K_1 (s^{-1})	R^2	K_1 (s^{-1})	R^2
Initial concentration ($mg·L^{-1}$)	20	0.00574	0.94685	0.02277	0.98289	0.00116	0.97861
	40	0.00259	0.92867	0.01492	0.98201	0.00124	0.96711
	60	0.00198	0.87693	0.01054	0.98165	0.00113	0.98023
	80	0.00185	0.85988	0.00921	0.89209	0.00162	0.90685
	100	0.00106	0.85759	0.01223	0.96441	0.00115	0.89644
Air inflow ($L·min^{-1}$)	0.5	0.00179	0.90235	0.02902	0.96762	0.00036	0.83429
	1.0	0.00259	0.92867	0.01492	0.98201	0.00065	0.96553
	1.5	0.00593	0.97738	0.02827	0.96705	0.00124	0.96711
	2.0	0.00465	0.93166	0.01777	0.98919	0.00156	0.97039

Table 1. *Cont.*

Conditions		Ozone Micro-Nano Bubbles				Ordinary Ozone Bubbles	
		Second-Order Kinetic (0–30 s)		First-Order Kinetic (30–120 s)		First-Order Kinetic (0–120 s)	
		K_2 ($mol^{-1}·L·s^{-1}$)	R^2	K_1 (s^{-1})	R^2	K_1 (s^{-1})	R^2
Initial pH	3	0.00314	0.98052	0.03072	0.98943	0.00111	0.88759
	5	0.00226	0.96461	0.02533	0.99193	0.00118	0.96597
	7	0.00259	0.92867	0.01492	0.98201	0.00124	0.96712
	9	0.00407	0.91711	0.01816	0.99495	0.00092	0.96833
	11	0.00145	0.87365	0.03039	0.98190	0.00095	0.96618

3.3. Impact of O_3-MNBs on Tetracycline Degradation Products

As shown in Figure 4a, the TOC removal performance of TC components under both aeration modes achieved reduction rates of 6.30% and 15.97%. The O_3-MNBs treatment yielded an average TOC removal of 11.01%, which was 41.69% higher than that of conventional ozone aeration. This deficient reduction of TOC suggests that the TC molecular structure was predominant over mineralization at this time scale [34,39]; hence, its organic carbon components primarily persisted in the aqueous phase like oxidation intermediates. Consequently, this evaluation needs further characterization of the composition of TC degradation products in water to elucidate the degradation pathways and mechanisms enabled by O_3-MNBs.

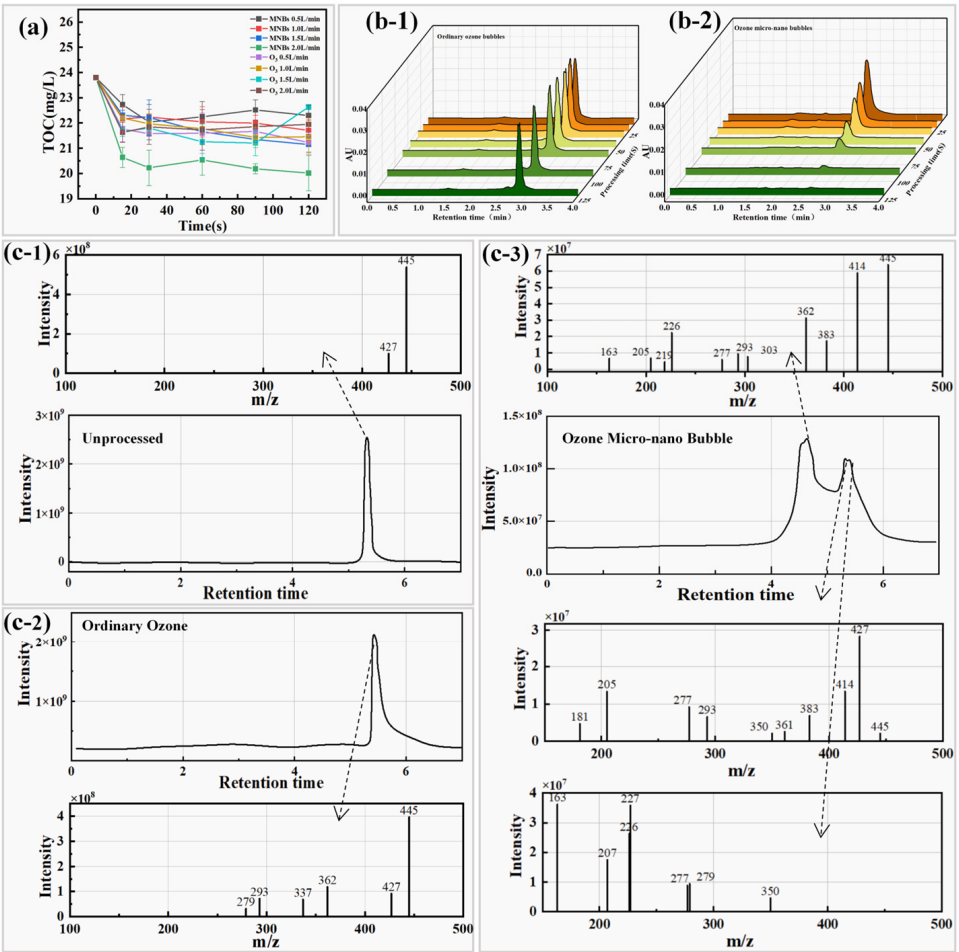

Figure 4. Tetracycline degradation products. (**a**) Removal of TOC from tetracycline solution using two types of ozone. (**b-1**,**b-2**) HPLC-UV test results of tetracycline solution treated with ozone. (**c-1**–**c-3**) LC-MS test results of tetracycline solution treated with ozone.

Figure 4(b-1,b-2) show the HPLC–UV chromatograms of TC solutions at different treatment times. These findings show that the peak distribution characteristics of the TC solutions differed markedly under the two ozone aeration conditions. For the conventional ozone aeration group, the TC peak height changed only slightly within 120 s of treatment, indicating that conventional ozone bubbles could not effectively degrade TC over a short time period. In contrast, in the O_3-MNBs group, the intensity of the TC peak gradually decreased, demonstrating that O_3-MNBs achieved significantly better TC removal than conventional ozone aeration, consistent with the results in Section 3.2. Additionally, new peaks appeared in the solution after O_3-MNB treatment; their intensities increased with reaction time, and their retention times were shorter than that of TC, which suggest the formation of more polar intermediate compounds during oxidation. To further elucidate the molecular structure distribution and transformation pathways of TC, liquid chromatography–mass spectrometry (LC–MS) analysis was conducted using an atmospheric-pressure chemical ionization (APCI) source. Under the optimal degradation conditions, a series of characteristic *m/z* fragments were detected, as shown in Figure 4(c-1–c-3).

As shown in Figure 4(c-3), during the oxidative degradation of organic pollutants, amino (—NH_2), carbonyl (—C=O), and hydroxyl (—OH) groups, as well as aromatic rings and C=C double bonds, are the primary attack sites of reactive oxidizing species. Figure 5 displays the ozone degradation of tetracycline inferred by proceeding via the following four pathways. In Pathway I, degradation initiates with a demethylation reaction, followed by ring cleavage and subsequent oxidation reactions, exhibiting various ketone and hydroxylated compounds. Throughout this process, singlet oxygen may participate in reactions with the C=C bonds in the molecule, triggering extensive ring cleavage and hydroxyl formation. Superoxide radicals act synergistically in this pathway, further promoting oxidation and reducing molecular weight. In Pathway II, degradation starts with oxidation of the N,N-dimethylamino group, accompanied by decarboxylation. Then, the reactive oxidizing species induce cleavage of the cyclic structure and further oxidation, yielding intermediate products containing multiple hydroxyl and carbonyl groups, which ultimately transform into low-molecular-weight alcohols and ketones. For Pathway III, degradation begins with demethylation and initial oxidation; under the sustained action of reactive oxidizing species, ring cleavage occurs, accompanied by the formation of new hydroxyl and carbonyl groups. In Pathway IV, Tetracycline is first converted into an intermediate product with *m/z* = 383, which subsequently undergoes demethylation and C–C single-bond cleavage to form a product with *m/z* = 207, and is finally further degraded into small-molecule compounds.

By jointly analyzing Figures 4(c-3) and 5, the TC degradation in the O_3-MNBs system included all the above pathways, but under conventional aeration, TC degradation occurred only via Pathway I and Pathway IV. Beyond the described pathways, these findings indicate that O_3-MNBs markedly expands radical-dominated, multi-branch degradation routes, driving intermediates to further evolve toward low *m/z* small molecules (e.g., *m/z* = 219/205/181/163). Therefore, the aromatic ring structures in TC are almost completely cleaved, while the dominant products are hydrophilic oxygenated small molecules, including short-chain carboxylic acids, aldehydes/ketones, and alcohols [40]. By contrast, conventional ozone aeration primarily follows the blue pathway, generating only a limited amount of partially oxidized products with relatively high *m/z*. This reaction remains largely at the level of functional-group modification and limited skeleton transformation, and cannot rapidly and continuously proceed to deep ring cleavage and mineralization. As a result, the degradation products still contain substantial aromatic-ring structures; no final small-molecule products were detected, indicating poor biodegradability and potential biotoxicity, and thus subsequent biological treatment would remain challenging [41]. By comparison, TC degradation by O_3-MNBs is more complete and the products are more

biodegradable, which, in principle, could substantially reduce the difficulty of downstream biological treatment and the associated biotoxicity risk [35].

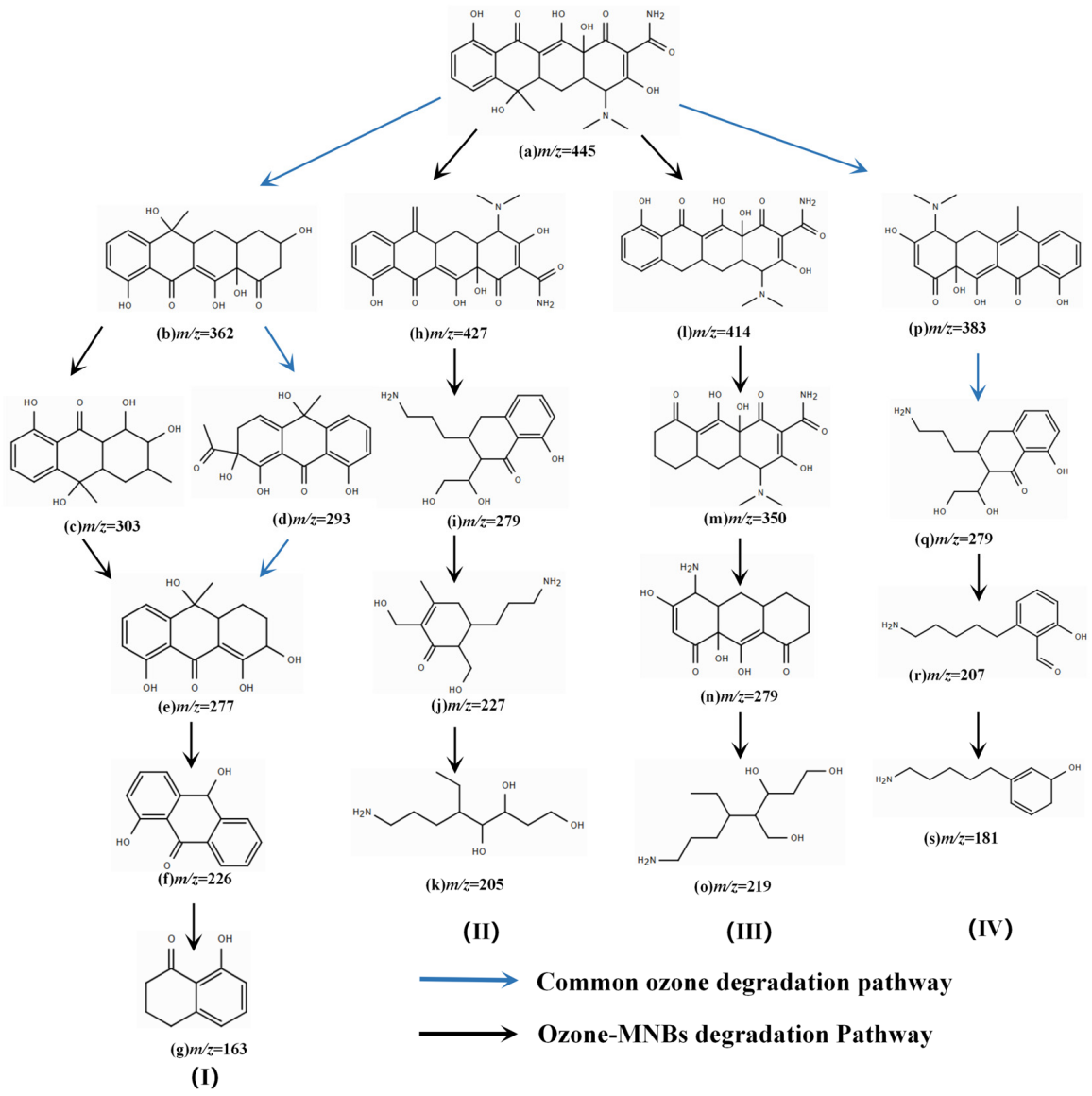

Figure 5. Tetracycline degradation pathway.

4. Discussion

TC antibiotics are ubiquitous in aquatic environments and continuously introduced, increasing the risk related to ecological toxicity and the spread of antimicrobial resistance; thus, there is an urgent need to develop efficient and risk-controllable removal strategies [35]. Although ozonation can rapidly transform various pharmaceutical micropollutants [42], it often exhibits "rapid parent compound disappearance but limited mineralization improvement" in TC systems. As a result, this method may reflect high removal efficiency, but the reduction risk may be deficient [43]. In response to that, O_3-MNBs have shown potential in promoting radical generation and mass-transfer capability, altering the formation of transformation intermediates, facilitating cleavage of aromatic-ring structures [44], and reducing biotoxicity in the products [43]. This study examines ozone stabilization in O_3-MNBs water and the mechanisms underlying efficient TC, highlighting the rapid reaction behavior of O_3-MNBs under conditions relevant to wastewater treatment.

Compared with other advanced oxidation processes for tetracycline (TC) removal, the O_3-MNBs process in this study provides a relatively simple but still highly effective oxidation route. Previous work has shown that adding H_2O_2 to conventional TC ozonation does not always markedly enhance TC disappearance [23], whereas electro-peroxone, photocatalytic, and photo-Fenton systems can promote deeper oxidation under optimized conditions; for example, a flow-through electro-peroxone process achieved TOC and COD removals of 44% and 65%, respectively [45], while photocatalytic and photo-Fenton systems have reported TC removals of about 95% and 94.7% within 60 min [46,47]. In comparison, the O_3-MNBs system in the present study achieved 96.25% TC removal within only 120 s, without requiring external H_2O_2 addition, iron salts, or solid catalysts, while also promoting deeper ring opening and skeletal fragmentation of intermediates. Therefore, these results provide a solid theoretical framework and technical support for applying O_3-MNBs technology to the treatment of TC-containing wastewaters. Its main engineering value may lie in reducing the parent antibiotic load, lowering the risk of toxic intermediates, and improving the biodegradability and treatability of the effluent before subsequent treatment. Although mineralization remained limited, O_3-MNBs appears particularly promising as a rapid pretreatment or polishing strategy for antibiotic-containing wastewaters. Further research is still required to assess the effects of real wastewater matrices, ozone utilization efficiency, energy consumption, off-gas management, and long-term stability during continuous operation.

4.1. Enhancing Stability of Ozone in Water by Micro-Nano Bubbles

This study demonstrated that, compared with conventional ozone aeration (Conv-O_3), O_3-MNBs significantly enhance ozone retention and mass-transfer efficiency in the aqueous phase. This improvement was fundamentally attributable to the high-density gas–liquid interfacial area. Thus, the bubble number concentration in the system reached the order of 10^7 mL^{-1}, with bubble diameters mainly distributed within 50–1200 nm, which markedly increases the specific interfacial area and strengthens ozone–water contact and mass-transfer flux [44]. Meanwhile, electrostatic repulsion arising from the negatively charged bubble surface (zeta potential of −4.71 to −13.65 mV) can suppress coalescence and premature collapse, prolonging bubble residence in the liquid phase and mitigating the insufficient effective contact caused by the rapid rise and escape of conventional large bubbles [48,49]. Furthermore, the Laplace pressure difference of MNBs increased the interfacial dissolution driving force, maintaining a locally supersaturated state [49,50]. Experimentally, the dissolved ozone concentration continued to rise for approximately 60 s after the gas supply ended; the peak ozone concentration was 85.5% higher than that under Conv-O_3, and the decay rate constant decreased by 39.6%. These findings indicate an "interfacial slow-release/storage effect" that can continuously replenish aqueous ozone after aeration stops and maintain a relatively high oxidant level. In addition, the ·OH concentration under O_3-MNBs was 117% higher than that under Conv-O_3, suggesting that interfacial activation and possible transient bubble-collapse events promoted ozone conversion via radical pathways [51]. Bubble size played an important role in determining the oxidation activity of the O_3-MNBs system. Under low gas flow rate conditions, the smaller bubbles generated provide a larger specific interfacial area, lower buoyancy-driven rising velocity, longer residence time, and higher Laplace pressure, thereby enhancing the dissolution and retention of ozone in water. However, the degradation performance in the present study was not controlled by bubble size alone; rather, it resulted from the combined influence of bubble size and ozone dosage. As gas inlet flow increased, bubble size also increased. Thus, the 1.5 L min^{-1} condition represented the best compromise between efficient oxidant supply and favorable gas–liquid interfacial characteristics, resulting in the highest dissolved ozone

concentration, ·OH generation. Overall, through the synergistic effects of high interfacial area, charge stabilization, Laplace-pressure-driven dissolution, and interfacial activation, O_3-MNBs significantly improve ozone mass transfer and aqueous-phase stability, providing a robust basis for subsequent rapid oxidation.

4.2. Efficient Degradation Mechanism of Tetracycline by O_3-MNBs

TC degradation in the O_3-MNB system exhibited a pronounced two-stage kinetic behavior. The initial stage (0–30 s) followed second-order kinetics, indicating that the reaction rate was jointly governed by the concentrations of both the oxidants (e.g., dissolved ozone and transiently generated ·OH) and TC, reflecting a very high level of reactive oxygen species in the early period. As the reaction proceeded, TC concentration decreased rapidly and the readily oxidizable sites were progressively consumed, while part of the reactive oxidants was also depleted through self-decomposition and side reactions with intermediates. The subsequent stage (30–120 s) followed first-order kinetics, suggesting that the reaction gradually shifted to a pseudo-first-order regime and became mainly controlled by the concentration of the remaining TC. In contrast, TC degradation under conventional ozone aeration followed first-order kinetics throughout [23], implying insufficient oxidant supply and persistence.

To clarify the specific contribution mechanisms of different active oxidation species in the O_3-MNB system to the degradation of TC, this study was verified by adding selective shielding agents. As shown in Figure S1, the degradation process is jointly driven by direct ozone oxidation, attack by ·OH, and the synergy of $\cdot O_2^-$, forming a coordinated system with multiple oxidation pathways operating in parallel. Furthermore, the reaction conditions further demonstrated the technical feasibility of the system by its optimization potential. Altogether, the reaction conditions further demonstrated the technical feasibility of the system by its optimization potential. Altogether, the degradation performance was regulated by the initial TC concentration, the ozone gas inlet flow rate, and solution pH. As the initial TC concentration increased from 20 to 100 mg·L^{-1}, the removal efficiency decreased from 97.26% to 93.30%, and the kinetic rate constants decreased accordingly; however, the absolute amount of TC removed increased markedly from 19.45 to 93.30 mg·L^{-1}, confirming the system's potential for treating high-strength pollutants. A prominent optimal ozone gas inlet flow rate was identified at 1.5 L·min^{-1}, at which the system achieved the best gas–liquid mass transfer balance and the highest removal efficiency (99.00%). Moreover, the system maintained high degradation performance over a wide pH range (3–11), with the highest final removal efficiencies (>98%) observed under strongly acidic and strongly alkaline conditions [36]. Under mildly alkaline conditions (pH = 9), the initial-stage reaction rate was the fastest, indicating that this environment favors ozone decomposition and triggers a rapid oxidation chain reaction dominated by radical pathways [52,53].

The formation pathways of degradation products and the degree of mineralization elucidate the chemical progression and limitations of the oxidation process. LC–MS results indicate that TC can vary via parallel pathways, including demethylation, decarboxylation, and aromatic ring division. Reactive oxygen species preferentially attack electron-rich sites (e.g., amino groups and phenolic hydroxyl groups), progressively generating intermediates with lower molecular weight and higher polarity [43]. It should be noted that the trends of parent TC removal and TOC reduction were not fully identical. The highest TC conversion at 1.5 L·min^{-1} indicates the optimum balance between ozone transfer and reactive oxygen species generation for rapid parent-compound destruction. By contrast, the slightly higher TOC reduction at 2.0 L·min^{-1} suggests that deeper oxidation of some transformation intermediates may benefit from a higher total ozone input. Although the overall TOC removal within the reaction time investigated in this study was deficient (an average of 11.01%

for O_3-MNBs), indicating that the process was dominated by structural transformation rather than complete mineralization, and showed a more diverse set of transformations. Moreover, O_3-MNBs could drive certain high *m/z* intermediates to further evolve toward low *m/z* small molecules, suggesting more extensive disruption of pharmacophores and polycyclic conjugated skeletons and an overall increase in product polarity [35]. In contrast, conventional ozone aeration tends to remain at the stage of functional-group modification and limited skeletal transformation, which may result in the persistence of relatively stable intermediates and increase uncertainty in subsequent treatment. Therefore, the advantages of O_3-MNBs are reflected not only in "faster degradation" but also in "more in-depth transformation, a stronger tendency toward lower-risk products, and improved suitability for downstream biological or advanced polishing processes".

As depicted in Figure 6, the proposed mechanistic schematic is summarized as a serial process, including mass transfer enhancement, followed by interface activation and multi-pathway synergistic oxidation. Specifically, MNBs enhance ozone dissolution and retention through their high specific interfacial area and Laplace-pressure-driven dissolution. At the gas–liquid interface and during possible transient bubble-collapse events, ozone is more readily converted into highly reactive species such as ·OH, forming a multi-oxidant network in which direct ozonation and radical-mediated oxidation proceed in parallel. This network can concurrently attack multiple susceptible sites on the TC molecule, enabling rapid degradation and structural destruction. Overall, this model systematically elucidates the intrinsic mechanism by which O_3-MNBs enhance TC degradation, providing a theoretical basis for applying O_3-MNBs to the treatment of refractory organic wastewater.

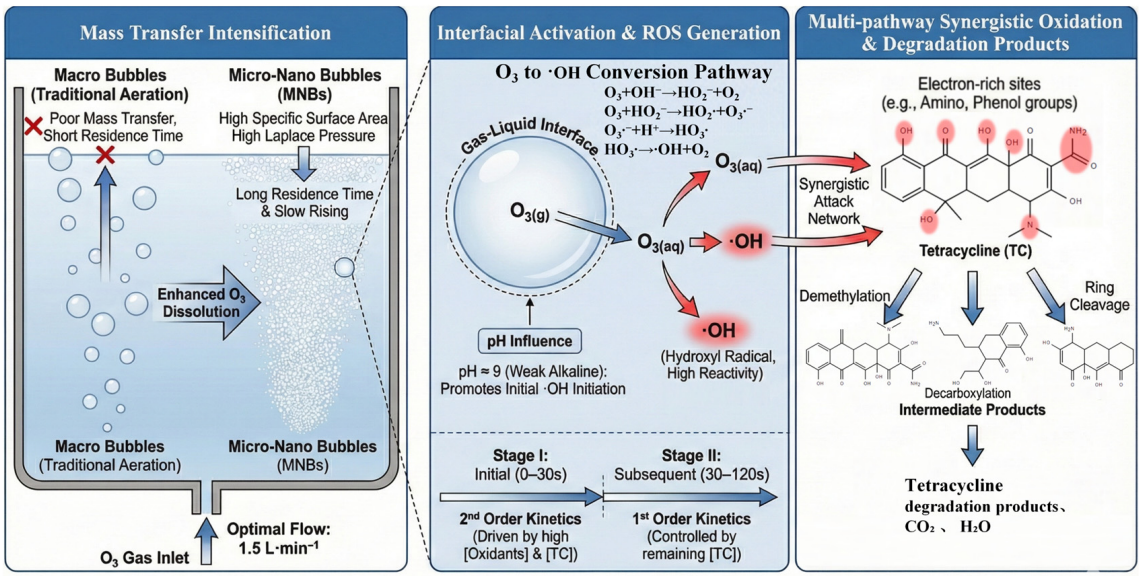

Figure 6. Schematic diagram of tetracycline degradation by O_3-MNBs.

5. Conclusions

This study systematically investigated the O_3-MNBs system in terms of ozone retention and mass transfer in the aqueous phase, TC degradation kinetics, transformation pathways, and the evolution of product profiles. Compared with conventional ozone aeration, O_3-MNBs exhibited clear advantages in sustaining oxidant availability and promoting deeper degradation of TC, demonstrating its scientific significance in improving ozone transfer, retention, and oxidation performance. Meanwhile, the results also indicate its potential for practical application, although further work is still needed to evaluate its performance in real wastewater matrices, clarify energy efficiency, and assess its feasibility in continuous-flow and larger-scale systems. The main conclusions are summarized as follows.

(1) The O_3-MNBs water exhibited a high bubble number concentration of (5.25–7.17) × 10^7 mL^{-1}, with more than 95% of bubbles distributed within 50–1200 nm. The maximum dissolved ozone concentration and radical concentration reached 27.9 $mg \cdot L^{-1}$ and 21.49 $\mu mol \cdot L^{-1}$, respectively, which were 86% and 117% higher than those obtained with conventional ozone sparging. These results demonstrate the superior gas–liquid mass transfer and oxidant activation capacity of the O_3-MNBs system.

(2) After aeration stopped, ozone decay in both systems followed first-order kinetics, but ozone persisted longer in the O_3-MNBs system. After 25 min, dissolved ozone in O_3-MNBs water remained at 4.69 $mg \cdot L^{-1}$, which was significantly higher than that in conventional ozonation. This indicates that O_3-MNBs can prolong oxidant availability and enhance the stability of ozone in water.

(3) O_3-MNBs achieved faster and more efficient TC degradation than conventional ozone aeration. The degradation process showed a two-stage kinetic behavior, with a rapid second-order stage during 0–30 s and a first-order stage during 30–120 s, whereas conventional ozonation followed first-order kinetics throughout the reaction. The apparent rate constant of conventional ozonation was only 7.14% of that of O_3-MNBs, confirming the marked kinetic advantage of the O_3-MNBs system.

(4) Compared with conventional ozonation, O_3-MNBs promoted broader radical-driven degradation pathways and facilitated the conversion of TC intermediates into lower-m/z small-molecule products through deeper ring opening and skeletal fragmentation. This suggests that O_3-MNBs has potential to improve the pretreatment of antibiotic-containing wastewater and reduce the burden on subsequent biological treatment.

Supplementary Materials: The following supporting information can be downloaded at: https://www.mdpi.com/article/10.3390/pr14071093/s1, Text S1: Chemical reagents; Text S2: MNBs preparation; Figure S1: Changes in tetracycline concentration after adding ROS inhibitors; Table S1: Summary of apparent ozone volumetric mass transfer coefficients under all conditions.

Author Contributions: Conceptualization, J.C.; Methodology, R.L. and T.W.; Validation, R.L.; Formal analysis, R.L. and C.Y.; Investigation, R.L.; Writing—original draft, R.L.; Writing—review & editing, T.W., H.Z. and F.M.; Supervision, T.W. All authors have read and agreed to the published version of the manuscript.

Funding: The study was supported by the Jing-Jin-Ji Regional Integrated Environmental Improvement-National Science and Technology Major Project (2025ZD1204600).

Data Availability Statement: The original contributions presented in this study are included in the article/Supplementary Material. Further inquiries can be directed to the corresponding author.

Conflicts of Interest: The authors declare no conflict of interest.

References

1. Rizzo, L.; Manaia, C.; Merlin, C.; Schwartz, T.; Dagot, C.; Ploy, M.C.; Michael, I.; Fatta-Kassinos, D. Urban wastewater treatment plants as hotspots for antibiotic resistant bacteria and genes spread into the environment: A review. *Sci. Total Environ.* **2013**, *447*, 345–360. [CrossRef] [PubMed]
2. Macedo, H.E.; Lehner, B.; A Nicell, J.; Khan, U.; Klein, E.Y. Antibiotics in the global river system arising from human consumption. *PNAS Nexus* **2025**, *4*, pgaf096. [CrossRef]
3. Larsson, D.J.; de Pedro, C.; Paxeus, N. Effluent from drug manufactures contains extremely high levels of pharmaceuticals. *J. Hazard. Mater.* **2007**, *148*, 751–755. [CrossRef]
4. Khan, G.A.; Berglund, B.; Khan, K.M.; Lindgren, P.-E.; Fick, J. Occurrence and abundance of antibiotics and resistance genes in rivers, canal and near drug formulation facilities—A study in Pakistan. *PLoS ONE* **2013**, *8*, e62712. [CrossRef]
5. Kuang, Y.; Guo, X.; Hu, J.; Li, S.; Zhang, R.; Gao, Q.; Yang, X.; Chen, Q.; Sun, W. Occurrence and risks of antibiotics in an urban river in northeastern Tibetan Plateau. *Sci. Rep.* **2020**, *10*, 20054. [CrossRef]

6. Zhang, F.; Mao, X.; Song, X.; Yu, H.; Yan, J.; Kong, D.; Liu, Y.; Yao, N.; Yang, S.; Xie, S.; et al. Ecological risks of antibiotics in urban wetlands on the Qinghai-Tibet Plateau, China. *Int. J. Environ. Res. Public Health* **2023**, *20*, 1735. [CrossRef]
7. Kergoat, L.; Besse-Hoggan, P.; Leremboure, M.; Beguet, J.; Devers, M.; Martin-Laurent, F.; Masson, M.; Morin, S.; Roinat, A.; Pesce, S.; et al. Environmental concentrations of sulfonamides can alter bacterial structure and induce diatom deformities in freshwater biofilm communities. *Front. Microbiol.* **2021**, *12*, 643719. [CrossRef]
8. Grenni, P. Antimicrobial Resistance in Rivers: A Review of the Genes Detected and New Challenges. *Environ. Toxicol. Chem.* **2022**, *41*, 687–714. [CrossRef]
9. Stanton, I.C.; Murray, A.K.; Zhang, L.; Snape, J.; Gaze, W.H. Evolution of antibiotic resistance at low antibiotic concentrations including selection below the minimal selective concentration. *Commun. Biol.* **2020**, *3*, 467. [CrossRef] [PubMed]
10. Amangelsin, Y.; Semenova, Y.; Dadar, M.; Aljofan, M.; Bjørklund, G. The Impact of Tetracycline Pollution on the Aquatic Environment and Removal Strategies. *Antibiotics* **2023**, *12*, 440. [CrossRef] [PubMed]
11. Xu, L.; Zhang, H.; Xiong, P.; Zhu, Q.; Liao, C.; Jiang, G. Occurrence, fate, and risk assessment of typical tetracycline antibiotics in the aquatic environment: A review. *Sci. Total. Environ.* **2021**, *753*, 141975. [CrossRef]
12. Pancu, D.F.; Scurtu, A.; Macasoi, I.G.; Marti, D.; Mioc, M.; Soica, C.; Coricovac, D.; Horhat, D.; Poenaru, M.; Dehelean, C. Antibiotics: Conventional therapy and natural compounds with antibacterial activity—A pharma-co-toxicological screening. *Antibiotics* **2021**, *10*, 401. [CrossRef]
13. Jiang, L.; Hu, X.; Yin, D.; Zhang, H.; Yu, Z. Occurrence, distribution and seasonal variation of antibiotics in the Huangpu River, Shanghai, China. *Chemosphere* **2011**, *82*, 822–828. [CrossRef]
14. Buxton, H.T.; Kolpin, D.W. Pharmaceuticals, Hormones, and Other Organic Wastewater Contaminants in US Streams. US Geological Survey. 2002. Available online: https://pubs.usgs.gov/publication/fs02702 (accessed on 7 January 2026).
15. Lundström, S.V.; Östman, M.; Bengtsson-Palme, J.; Rutgersson, C.; Thoudal, M.; Sircar, T.; Blanck, H.; Eriksson, K.M.; Tysklind, M.; Flach, C.-F.; et al. Minimal selective concentrations of tetracycline in complex aquatic bacterial biofilms. *Sci. Total. Environ.* **2016**, *553*, 587–595. [CrossRef] [PubMed]
16. Larsson, D.J.; Flach, C.-F. Antibiotic resistance in the environment. *Nat. Rev. Microbiol.* **2022**, *20*, 257–269. [CrossRef]
17. Shutter, M.C.; Akhondi, H. Tetracycline. In *StatPearls*; StatPearls Publishing: Treasure Island, FL, USA, 2025. Available online: http://www.ncbi.nlm.nih.gov/books/NBK549905/ (accessed on 7 January 2026).
18. Li, B.; Zhang, T. Removal mechanisms and kinetics of trace tetracycline by two types of activated sludge treating freshwater sewage and saline sewage. *Environ. Sci. Pollut. Res.* **2013**, *20*, 3024–3033. [CrossRef] [PubMed]
19. Zhong, S.-F.; Yang, B.; Lei, H.-J.; Xiong, Q.; Zhang, Q.-Q.; Liu, F.; Ying, G.-G. Transformation products of tetracyclines in three typical municipal wastewater treatment plants. *Sci. Total. Environ.* **2022**, *830*, 154647. [CrossRef] [PubMed]
20. Ahmed, N.; Vione, D.; Rivoira, L.; Carena, L.; Castiglioni, M.; Bruzzoniti, M.C. A review on the degradation of pollutants by fenton-like systems based on zero-valent iron and persulfate: Effects of reduction potentials, pH, and anions occurring in waste waters. *Molecules* **2021**, *26*, 4584. [CrossRef]
21. Gopal, G.; Alex, S.A.; Chandrasekaran, N.; Mukherjee, A. A review on tetracycline removal from aqueous systems by advanced treatment techniques. *RSC Adv.* **2020**, *10*, 27081–27095. [CrossRef]
22. Ikehata, K.; Naghashkar, N.J.; El-Din, M.G. Degradation of Aqueous Pharmaceuticals by Ozonation and Advanced Oxidation Processes: A Review. *Ozone Sci. Eng.* **2006**, *28*, 353–414. [CrossRef]
23. Wang, Y.; Zhang, H.; Zhang, J.; Lu, C.; Huang, Q.; Wu, J.; Liu, F. Degradation of tetracycline in aqueous media by ozonation in an internal loop-lift reactor. *J. Hazard. Mater.* **2011**, *192*, 35–43. [CrossRef] [PubMed]
24. Wu, J.; Jiang, Y.; Zha, L.; Ye, Z.; Zhou, Z.; Ye, J.; Zhou, H. Tetracycline degradation by ozonation, and evaluation of biodegradability and toxicity of ozonation byproducts. *J. Environ. Eng. Sci.* **2013**, *8*, 580–586. [CrossRef]
25. Zhang, J.; Yang, L.; Liu, C.; Ma, J.; Yan, C.; Mu, S.; Yu, M. Efficient degradation of tetracycline hydrochloride wastewater by microbubble catalytic ozonation with sludge biochar-loaded layered polymetallic hydroxide. *Sep. Purif. Technol.* **2024**, *340*, 126767. [CrossRef]
26. Gao, J.; Chen, S.; Gao, Y.; Sun, W.; Zhou, J.; Shah, K.J.; Sun, Y. Current Developments in Ozone Catalyst Preparation Techniques and Their Catalytic Oxidation Performance. *Catalysts* **2025**, *15*, 671. [CrossRef]
27. Tang, S.; Yuan, D.; Zhang, Q.; Liu, Y.; Liu, Z.; Huang, H. Fe-Mn bi-metallic oxides loaded on granular activated carbon to enhance dye removal by catalytic ozonation. *Environ. Sci. Pollut. Res.* **2016**, *23*, 18800–18808. [CrossRef]
28. Zhao, S.; Wu, J.; Li, Y. Advances in the research on the properties and applications of micro-nano bubbles. *Processes* **2025**, *13*, 2106. [CrossRef]
29. Hernandez-Alvarado, F.; Kalaga, D.V.; Turney, D.; Banerjee, S.; Joshi, J.B.; Kawaji, M. Void fraction, bubble size and interfacial area measurements in co-current downflow bubble column reactor with microbubble dispersion. *Chem. Eng. Sci.* **2017**, *168*, 403–413. [CrossRef]
30. Seridou, P.; Kalogerakis, N. Disinfection applications of ozone micro- and nanobubbles. *Environ. Sci. Nano* **2021**, *8*, 3493–3510. [CrossRef]

31. Takahashi, M.; Chiba, K.; Li, P. Formation of Hydroxyl Radicals by Collapsing Ozone Microbubbles under Strongly Acidic Conditions. *J. Phys. Chem. B* **2007**, *111*, 11443–11446. [CrossRef]
32. Zhou, Y.; Cao, D.; Zhang, X. Degradation mechanism of micro-nanobubble technology for organic pollutants in aqueous solutions. *Nanomaterials* **2022**, *12*, 2654. [CrossRef]
33. Xiao, W.; Zhang, H.; Wang, X.; Wang, B.; Long, T.; Deng, S.; Yang, W. Interaction mechanisms and application of ozone micro/nanobubbles and nanoparticles: A review and perspective. *Nanomaterials* **2022**, *12*, 1958. [CrossRef] [PubMed]
34. Wang, C.; Lin, C.-Y.; Liao, G.-Y. Feasibility Study of Tetracycline Removal by Ozonation Equipped with an Ultrafine-Bubble Compressor. *Water* **2021**, *13*, 1058. [CrossRef]
35. Tang, L.; Huang, J.; Zhuang, C.; Zhou, S.; Sun, L.; Lu, H. Micronano-bubble ozonation as an efficient pretreatment technology for raw oxytetracycline production wastewater discharged to biological treatment. *Chem. Eng. J.* **2023**, *476*, 146518. [CrossRef]
36. Zhao, K.; Padervand, M.; Ren, H.; Jia, T.; Guo, Q.; Yang, L.; Wang, C. Enhancing Tetracycline Removal Efficiency through Ozone Micro–Nano Bubbles: Environmental Implication and Degradation Pathway. *ACS EST Eng.* **2024**, *4*, 1860–1870. [CrossRef]
37. Yang, Z.-C.; Peng, L.; Jing, Z.-B.; Wang, W.-L.; Cai, H.-Y.; Jiang, Y.-Q.; Li, L.-D.; Ye, B.; Wu, Q.-Y. Superior water disinfection via ozone micro-bubble aeration: Performance and mechanism. *J. Hazard. Mater.* **2025**, *492*, 138174. [CrossRef]
38. Wang, X.; Zhu, T.; Duan, H.; Jiang, J.; Lu, X.; Yang, Y. Mechanistic insights into hydroxyl ion-driven ozone activation at nanobubble interfaces for enhanced pollutant degradation. *Chem. Eng. J.* **2025**, *519*, 165373. [CrossRef]
39. Hossain, A.; Nishimura, Y.; Salma, U.; Tokumura, M.; Nishino, T.; Raknuzzaman, M.; Noro, K.; Watanabe, K.; Amagai, T.; Makino, M. Effects of water matrices on the removal of oxytetracycline antibiotic and total organic carbon (TOC) using four different oxidation processes. *Results Eng.* **2024**, *24*, 103183. [CrossRef]
40. Koundle, P.; Nirmalkar, N.; Momotko, M.; Makowiec, S.; Boczkaj, G. Tetracycline degradation for wastewater treatment based on ozone nanobubbles advanced oxidation processes (AOPs)—Focus on nanobubbles formation, degradation kinetics, mechanism and effects of water composition. *Chem. Eng. J.* **2024**, *501*, 156236. [CrossRef]
41. Lim, S.; Shi, J.L.; von Gunten, U.; McCurry, D.L. Ozonation of organic compounds in water and wastewater: A critical review. *Water Res.* **2022**, *213*, 118053. [CrossRef]
42. Lee, Y.; Gerrity, D.; Lee, M.; Bogeat, A.E.; Salhi, E.; Gamage, S.; Trenholm, R.A.; Wert, E.C.; Snyder, S.A.; von Gunten, U. Prediction of Micropollutant Elimination during Ozonation of Municipal Wastewater Effluents: Use of Kinetic and Water Specific Information. *Environ. Sci. Technol.* **2013**, *47*, 5872–5881. [CrossRef]
43. Khan, M.H.; Bae, H.; Jung, J.-Y. Tetracycline degradation by ozonation in the aqueous phase: Proposed degradation intermediates and pathway. *J. Hazard. Mater.* **2010**, *181*, 659–665. [CrossRef]
44. Hu, L.; Xia, Z. Application of ozone micro-nano-bubbles to groundwater remediation. *J. Hazard. Mater.* **2018**, *342*, 446–453. [CrossRef]
45. Zhang, Y.; Zuo, S.; Zhang, Y.; Ren, G.; Pan, Y.; Zhang, Q.; Zhou, M. Simultaneous removal of tetracycline and disinfection by a flow-through electro-peroxone process for reclamation from municipal secondary effluent. *J. Hazard. Mater.* **2019**, *368*, 771–777. [CrossRef] [PubMed]
46. Jia, X.; Wang, F.; Xu, X.; Liu, C.; Zhang, L.; Jiao, S.; Zhu, G.; Wang, X.; Yu, G. Highly Efficient Photocatalytic Degradation of Tetracycline by Modifying UiO-66 via Different Regulation Strategies. *ACS Omega* **2023**, *8*, 27375–27385. [CrossRef]
47. Li, D.; Zhu, Z.; Yin, C.; Xu, F. Enhanced photo-fenton degradation of tetracycline hydrochloride using type-II magnetic FeP/Cu2O heterojunction catalysts. *Surf. Interfaces* **2025**, *75*, 107766. [CrossRef]
48. Nirmalkar, N.; Pacek, A.W.; Barigou, M. On the Existence and Stability of Bulk Nanobubbles. *Langmuir* **2018**, *34*, 10964–10973. [CrossRef] [PubMed]
49. Lasek, L.; Krzywanski, J.; Skrobek, D.; Zylka, A.; Nowak, W. Review of micro-and nanobubble technologies: Advancements in theory and applications and perspectives on adsorption cooling and desalination systems. *Energies* **2023**, *16*, 8078. [CrossRef]
50. Zhang, H.; Guo, Z.; Zhang, X. Surface enrichment of ions leads to the stability of bulk nanobubbles. *Soft Matter* **2020**, *16*, 5470–5477. [CrossRef]
51. Yang, S.-Y.; Wang, W.; Chen, J.-J.; Francisco, J.S.; Liu, X.-W. Probing catalyst-free hydroxyl radical generation at microbubble interfaces. *Nat. Commun.* **2025**, *16*, 8835. [CrossRef]
52. Elovitz, M.S.; von Gunten, U.; Kaiser, H.-P. Hydroxyl Radical/Ozone Ratios During Ozonation Processes. II. The Effect of Temperature, pH, Alkalinity, and DOM Properties. *Ozone Sci. Eng.* **2000**, *22*, 123–150. [CrossRef]
53. Buffle, M.-O.; Schumacher, J.; Meylan, S.; Jekel, M.; von Gunten, U. Ozonation and Advanced Oxidation of Wastewater: Effect of O_3Dose, pH, DOM and $HO^{\bullet}$-Scavengers on Ozone Decomposition and $HO^{\bullet}$ Generation. *Ozone Sci. Eng.* **2006**, *28*, 247–259. [CrossRef]

Disclaimer/Publisher's Note: The statements, opinions and data contained in all publications are solely those of the individual author(s) and contributor(s) and not of MDPI and/or the editor(s). MDPI and/or the editor(s) disclaim responsibility for any injury to people or property resulting from any ideas, methods, instructions or products referred to in the content.